

# Evolution of entanglement entropy in strongly correlated bosons in an optical lattice

Shion Yamashika,<sup>1,\*</sup> Daichi Kagamihara,<sup>2</sup> Ryosuke Yoshii,<sup>3</sup> and Shunji Tsuchiya<sup>1</sup>

<sup>1</sup>*Department of Physics, Chuo University, Bunkyo, Tokyo 112-8551, Japan*

<sup>2</sup>*Department of Physics, Kindai University, Higashi-Osaka, Osaka 577-8502, Japan*

<sup>3</sup>*Center of Liberal Arts and Sciences, Sanyo-Onoda City University, Yamaguchi 756-0884, Japan*

(Dated: October 5, 2022)

We study the time evolution of entanglement entropy of bosons in a one-dimensional optical lattice induced by a sudden quench of the hopping amplitude  $J$ . We consider the system being quenched into the deep Mott-insulating (MI) regime, i.e.,  $J/U \ll 1$  ( $U$  is the strength of the on-site repulsive interaction), from the product state with individual boson isolated in each lattice site. The low-energy excited states in this regime can be effectively described by fermionic quasiparticles known as doublons and holons. Developing the effective theory, we analytically calculate the time evolution of the second-order Rényi entropy (RE) for a subsystem and propose a quasiparticle picture for the time evolution of the RE based on the obtained analytic expressions. Doublons and holons are excited by the quench as entangled pairs that propagate with the velocity  $v_{\text{pair}} = 6J$ . The RE reflects the population of doublon-holon pairs that span the boundary of the subsystem. In the short-time scale [ $Jt/\hbar = \mathcal{O}(1)$ ], the RE exhibits the rapid oscillations with the frequency  $U/\hbar$ , while in the long-time scale ( $Jt/\hbar \gg 1$ ) the RE grows linearly in time until the pair spreads beyond the size of the subsystem and the RE saturates to a constant. We derive the growth rate of the RE and analytically show that the constant value of RE after the saturation obeys the volume-law scaling.

## I. INTRODUCTION

Entanglement is one of the most intriguing notions of quantum mechanics. It describes non-local correlations incompatible with local realism [1], which is clearly demonstrated by the violation of the Bell inequality [2]. Understanding its role in quantum many-body systems is crucial for fundamental problems in diverse fields, such as thermalization in an isolated many-body system [3–8] and the Hawking radiation from a black hole [9, 10]. Moreover, entangled many-body systems have wide applications including fault-tolerant quantum computation [11, 12].

Entanglement between quantum objects can be quantified by entanglement entropy. It has been a major subject of theoretical investigation in quantum many-body systems, as well as in quantum field theories. In particular, dynamics of entanglement entropy in integrable systems has been intensively investigated [13–16] since the pioneering work by Calabrese and Cardy [17, 18].

Despite recent developments of experimental techniques, measuring entanglement entropy remains challenging. A great advance has been recently made in the system of ultracold bosonic atoms in an optical lattice. The second-order Rényi entropy (RE), which is one of the measures of entanglement entropy, has been successfully measured by preparing two independent systems in the same state, letting them interfere, and counting the number parity of atoms in each lattice site by an atomic gas microscope [19, 20]. Furthermore, the time evolution of RE after a sudden quench of atomic hopping has been observed in the superfluid (SF) regime by using this technique [21].

In this paper, motivated by the experiments [20, 21], we study the quench dynamics of entanglement entropy of bosons in a one-dimensional optical lattice with unit filling. Our main focus is on the quench dynamics of RE in the deep Mott insulating (MI) regime. The low-energy dynamics in this regime can be effectively described by fermionic quasiparticles referred to as a doublon and a holon, which correspond to an excess particle and a hole on top of the unit filling, respectively [22]. We develop the effective theory and derive the analytical expressions for the time-evolving RE after the quench. We propose a physical picture for the time-evolution of RE in terms of quasiparticles based on the analytical expressions. We further compare it with the quasiparticle picture for the long-time dynamics of entanglement entropy in an integrable system proposed by Calabrese and Cardy [18].

The organization of the paper is as follows: In Sec. II, we explain the model and setup for the quench dynamics of bosons in an optical lattice and introduce the RE. In Sec. III, we introduce the effective theory in the deep MI regime. In Sec. IV, we study RE for the ground state. In Sec. V, we study the time evolution of RE after the quench. In Sec. VI, we argue the physical picture for the time evolution of the RE. Finally, in Sec. VII, we discuss the validity of the effective theory and experimental verifiability of our results. We set  $\hbar = 1$  and take the lattice constant to be unity throughout this paper.

## II. MODEL AND SETUP

We consider bosons in a one-dimensional (1D) optical lattice at zero temperature. When the lattice potential is deep enough, the system is well described by the Bose-

\* shion8ma4ka@icloud.com

Hubbard model (BHM) [23–25]

$$\hat{H} = -J \sum_j (\hat{b}_j^\dagger \hat{b}_{j+1} + \text{h.c.}) + \frac{U}{2} \sum_j \hat{n}_j (\hat{n}_j - 1), \quad (1)$$

where  $\hat{b}_j$  ( $\hat{b}_j^\dagger$ ) denotes the annihilation (creation) operator of a boson on the  $j$ th site and  $\hat{n}_j = \hat{b}_j^\dagger \hat{b}_j$  is the number operator.  $J$  denotes the hopping amplitude between nearest-neighbor sites and  $U > 0$  is the strength of the on-site repulsive interaction. We assume the periodic boundary condition.

The 1D BHM exhibits a quantum phase transition between the SF and MI phases [26–32]: When the total number of bosons  $N$  is commensurate with the number of total sites  $L$ , the ground state is in the SF phase for small  $U/J$ , while it is in the MI phase for large  $U/J$ . The SF-MI phase transition of the Kosterlitz-Thouless type occurs at  $U/J \simeq 3.28$  for unit filling ( $N/L = 1$ ) [29–32]. The ground state is in the SF phase when  $N$  is incommensurate with  $L$  irrespective of the values of  $U$  and  $J$ .

Suppose the whole system consists of the subsystems A and B. The RE for the subsystem A is defined as [33]

$$S_A = -\log[\text{tr}_A(\hat{\rho}_A^2)], \quad (2)$$

where  $\hat{\rho}$  and  $\hat{\rho}_A = \text{tr}_B(\hat{\rho})$  are the density matrices for the whole system and the subsystem A, respectively.  $\text{tr}_{B(A)}$  stands for trace over the subsystem B (A).  $\text{tr}_A(\hat{\rho}_A^2)$  quantifies the purity of the subsystem A [34]:  $\text{tr}_A(\hat{\rho}_A^2) = 1$  when the subsystem A is a pure state, while  $\text{tr}_A(\hat{\rho}_A^2) < 1$  when it is a mixed state. When the subsystems A and B have no entanglement,  $\rho_A$  becomes a pure state and we obtain  $S_A = 0$ . When the subsystem A and B are entangled,  $\rho_A$  becomes a mixed state and we obtain  $S_A > 0$ .

We follow the quench protocol of the experiments [20–22]. Namely, individual atom is initially localized in a single lattice well by a deep lattice potential. At the initial time ( $t = 0$ ) tunneling of atoms is abruptly switched on by lowering the lattice depth and the system evolves following the Hamiltonian (1) as  $|\psi(t)\rangle = e^{-i\hat{H}t}|\psi_0\rangle$ .

The initial state can be written as

$$|\psi_0\rangle = \prod_{j=1}^L \hat{b}_j^\dagger |0\rangle_j, \quad (3)$$

where  $|\nu\rangle_j$  ( $\nu = 0, 1, 2, \dots$ ) denote the Fock states with  $\nu$  atoms on the  $j$ th site. It corresponds to the ground state of the MI limit ( $J/U = 0$ ). Since the initial state (3) is a product state,  $S_A = 0$  at  $t = 0$ .  $S_A$  grows in time after the quench as tunneling bosons create entanglement between the subsystems.

### III. EFFECTIVE THEORY IN THE DEEP MI REGIME

We assume that the lattice potential is slightly lowered and the value of  $J/U$  is set in the deep MI regime ( $J/U \ll$

1) at  $t > 0$ . The low-energy excited states in this regime can be described in terms of doublons and holons [22]. Given that such a weak perturbation associated with the quench involves only low-energy excited states, the time evolution of the system after the quench is considered well described by the effective theory. The Hamiltonian for the effective theory reads [22]

$$\begin{aligned} \hat{H}_{\text{eff}} = & -J \sum_j [2\hat{d}_j^\dagger \hat{d}_{j+1} + \hat{h}_{j+1}^\dagger \hat{h}_j \\ & + \sqrt{2}(\hat{d}_j^\dagger \hat{h}_{j+1}^\dagger - \hat{h}_j \hat{d}_{j+1}) + \text{h.c.}] \\ & + \frac{U}{2} \sum_j (\hat{d}_j^\dagger \hat{d}_j + \hat{h}_j^\dagger \hat{h}_j), \end{aligned} \quad (4)$$

where  $\hat{d}_j$  ( $\hat{d}_j^\dagger$ ) and  $\hat{h}_j$  ( $\hat{h}_j^\dagger$ ) denote the fermionic annihilation (creation) operators for doublon and holon, respectively. We give a derivation of  $\hat{H}_{\text{eff}}$  and its Fourier transformed form in Appendix A.

The quadratic Hamiltonian  $\hat{H}_{\text{eff}}$  can be diagonalized by the Bogoliubov transformation

$$\begin{pmatrix} \hat{\gamma}_{d,k} \\ \hat{\gamma}_{h,-k}^\dagger \end{pmatrix} = \begin{pmatrix} u_k & -iv_k \\ -iv_k & u_k \end{pmatrix} \begin{pmatrix} \hat{d}_k \\ \hat{h}_{-k}^\dagger \end{pmatrix}, \quad (5)$$

where

$$u_k = \sqrt{\frac{1}{2} \left( 1 + \frac{f_{d,k} + f_{h,k}}{\sqrt{(f_{d,k} + f_{h,k})^2 + 4g_k^2}} \right)}, \quad (6)$$

$$v_k = \text{sgn}(k) \sqrt{\frac{1}{2} \left( 1 - \frac{f_{d,k} + f_{h,k}}{\sqrt{(f_{d,k} + f_{h,k})^2 + 4g_k^2}} \right)}. \quad (7)$$

$\hat{\gamma}_{d,k}$  and  $\hat{\gamma}_{h,k}$  denote the annihilation operators of quasi-particles, which we refer to as ‘‘bogolons’’ hereafter. Substituting Eq. (5) into Eq. (A15),  $\hat{H}_{\text{eff}}$  is diagonalized as

$$\hat{H}_{\text{eff}} = \sum_k (\epsilon_{d,k} \hat{\gamma}_{d,k}^\dagger \hat{\gamma}_{d,k} + \epsilon_{h,k} \hat{\gamma}_{h,-k}^\dagger \hat{\gamma}_{h,-k}), \quad (8)$$

where the dispersions of bogolons are given by

$$\epsilon_{d,k} = -J \cos(k) + \frac{1}{2} \sqrt{[U - 6J \cos(k)]^2 + 32J^2 \sin^2(k)}, \quad (9)$$

$$\epsilon_{h,k} = J \cos(k) + \frac{1}{2} \sqrt{[U - 6J \cos(k)]^2 + 32J^2 \sin^2(k)}. \quad (10)$$

They have energy gap  $\epsilon_{d,k=0} = U/2 - 4J$  and  $\epsilon_{h,k=0} = U/2 - 2J$ . The ground state  $|\text{vac}\rangle$  that satisfies  $\hat{\gamma}_{d,k}|\text{vac}\rangle = \hat{\gamma}_{h,k}|\text{vac}\rangle = 0$  is given as

$$|\text{vac}\rangle = \prod_k [u_k + iv_k \hat{d}_k^\dagger \hat{h}_{-k}^\dagger] |\psi_0\rangle. \quad (11)$$

It has a similar form with the BCS wave function [35]. It shows that doublon-holon pairs similar to the Cooper pairs are condensed in the ground state.

The time-evolving wave function after the quench is given as

$$\begin{aligned} |\psi(t)\rangle &= e^{-i\hat{H}_{\text{eff}}t}|\psi_0\rangle \\ &= \prod_k [u_k - iv_k e^{-i(\epsilon_{d,k} + \epsilon_{h,k})t} \hat{\gamma}_{d,k}^\dagger \hat{\gamma}_{h,-k}^\dagger] |\text{vac}\rangle. \end{aligned} \quad (12)$$

It illustrates that pairs of bogolons are excited by the quench. We employ Eq. (12) to calculate the time evolution of RE.

#### IV. RÉNYI ENTROPY FOR THE GROUND STATE

Let us first evaluate RE for the ground state (11) before studying its time evolution. Since Eq. (11) is a ground state of a quadratic Hamiltonian, i.e., a Gaussian state, RE can be evaluated from the single-particle correlation functions [36]. We summarize the calculation of RE for a Gaussian state in Appendix B.

Evaluating the single-particle correlation functions in Eqs. (B5) and (B6) by  $|\text{vac}\rangle$ , we obtain  $C_{dh} = C_{hd} = 0$ ,  $F_{dd} = F_{hh} = 0$ , and

$$[C_{dd}]_{ij} = [C_{hh}]_{ij} = \frac{1}{L} \sum_k v_k^2 e^{ik(i-j)}, \quad (13)$$

$$[F_{dh}]_{ij} = [F_{hd}]_{ij} = \frac{i}{L} \sum_k u_k v_k e^{ik(i-j)}. \quad (14)$$

Note that  $C_{ij} = \mathcal{O}((J/U)^2)$ ,  $F_{ij} = \mathcal{O}(J/U)$ , and  $F_{ij} = -F_{ji}$ . The matrix of the single-particle correlation functions  $M$  in Eq. (B4) can be simplified as (we omit the indices  $d$  and  $h$ )

$$M = \begin{pmatrix} I - C & 0 & 0 & F \\ 0 & I - C & F & 0 \\ 0 & -F & C & 0 \\ -F & 0 & 0 & C \end{pmatrix}. \quad (15)$$

From above, we obtain

$$\text{tr}[(M)^2] = 2L_A - 4\text{tr}(C) + 4\|F\|_F^2 + \mathcal{O}((J/U)^4), \quad (16)$$

where  $\|O\|_F = \sqrt{\sum_{ij} |O_{ij}|^2}$  denotes the Frobenius norm. Using Eq. (B7), another form can be derived as

$$\text{tr}[(M)^2] = 2L_A - 2 \sum_{\alpha=1}^{2L_A} [f_\alpha - (f_\alpha)^2]. \quad (17)$$

Comparing Eqs. (16) and (17), we obtain

$$\sum_{\alpha=1}^{2L_A} [f_\alpha - (f_\alpha)^2] = 2 \left[ \text{tr}(C) - \|F\|_F^2 \right] + \mathcal{O}((J/U)^4) \quad (18)$$

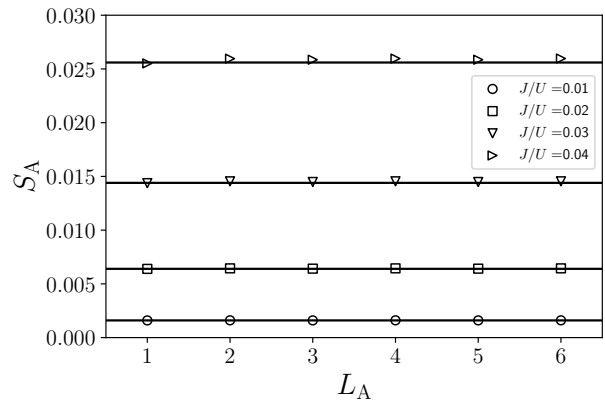


FIG. 1. RE for the ground state  $|\text{vac}\rangle$ . The symbols indicate the numerical data of the iTEBD calculations. The analytic results of Eq. (22) are indicated by the horizontal solid lines.

Substituting Eq. (18) into Eq. (B3), we obtain

$$S_A = 4 \left[ \text{tr}(C) - \|F\|_F^2 \right] + \mathcal{O}((J/U)^4). \quad (19)$$

In the limit  $L \rightarrow \infty$ , replacing the summations over  $k$  with integrals  $[\sum_k \rightarrow (L/2\pi) \int_{-\pi}^{\pi} dk]$  in Eqs. (13) and (14), we obtain

$$\text{tr}(C) = 4(J/U)^2 L_A + \mathcal{O}((J/U)^4), \quad (20)$$

$$\|F\|_F^2 = 4(J/U)^2 (L_A - 1) + \mathcal{O}((J/U)^3). \quad (21)$$

From (19), we finally arrive at a simple expression

$$S_A = 16(J/U)^2 + \mathcal{O}((J/U)^3). \quad (22)$$

The above expression clearly shows that  $S_A$  is independent of the subsystem size and therefore follows the *area-law scaling*, which is a characteristic feature of the ground state of a gapped system [37]. Notice that the first term in Eq. (22) arises from  $\|F\|_F^2$ , where  $F$  is an anomalous correlation function of doublon-holon pairs. The area-law scaling thus originates from the condensed doublon-holon pairs.

We calculate the ground state wave function of the BHM (1) numerically by imaginary-time evolution using the infinite time-evolving block-decimation (iTEBD) algorithm [38] and evaluate RE with it. Figure 1 shows that the numerical results of the iTEBD calculations agree well with Eq. (22).

#### V. DYNAMICS OF RÉNYI ENTROPY

In this section, we study the time evolution of RE. We calculate RE for a single site ( $L_A = 1$ ) in Sec. V A using the general properties of the density matrix. We further calculate RE for  $L_A \geq 1$  in Sec. V B by extending the formalism in Appendix B. We argue the characteristic features of the RE and their physical picture.

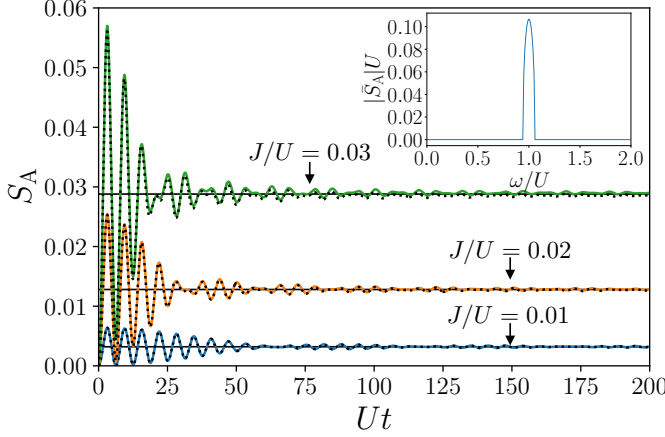


FIG. 2. Time evolution of the RE for a single site ( $L_A = 1$ ). Equation (29) is plotted as the solid lines. The horizontal lines indicate the asymptotic values  $S_A(t \rightarrow \infty) = 32(J/U)^2$ . The dotted lines indicate the numerical results of the iTEBD calculations. The inset shows the Fourier transform  $\bar{S}_A(\omega)$  in Eq. (32).

### A. Rényi entropy for a single site

The reduced density matrix for a single-site  $j(= A)$  can be written as

$$\hat{\rho}_A = \sum_{m,n \in \{0,1,2\}} r_{mn} |m\rangle_j \langle n|. \quad (23)$$

We take  $r_{11}$ ,  $r_{22}$ ,  $r_{01}$ ,  $r_{02}$ , and  $r_{12}$  as independent parameters from the conditions  $\text{tr}_A(\hat{\rho}_A) = 1$  and  $\hat{\rho}_A^\dagger = \hat{\rho}_A$ .  $r_{00}$  and  $r_{22}$  are equivalent to the densities of holon and doublon, respectively, as

$$r_{00} = \langle 0|_j \hat{\rho}_A |0\rangle_j \simeq \text{tr}_A(h_j \hat{\rho}_A h_j^\dagger) = \langle \hat{n}_{jh} \rangle, \quad (24)$$

$$r_{22} = \langle 2|_j \hat{\rho}_A |2\rangle_j \simeq \text{tr}_A(d_j \hat{\rho}_A d_j^\dagger) = \langle \hat{n}_{jd} \rangle, \quad (25)$$

where  $\hat{n}_{jh} = \hat{h}_j^\dagger \hat{h}_j$  and  $\hat{n}_{jd} = \hat{d}_j^\dagger \hat{d}_j$ . Using Eq. (12), we find that doublons and holons have the same density  $r_{00} = r_{22} = r(t)$ , where

$$r(t) = \frac{2}{L} \sum_k u_k^2 v_k^2 \{1 - \cos[(\epsilon_{d,k} + \epsilon_{h,k})t]\}. \quad (26)$$

Since all the doublons and holons are excited in doublon-holon pairs in  $|\psi(t)\rangle$  [See Eq. (29)], the densities of doublons and holons are equal and the off-diagonal elements vanishes, i.e.,  $r_{01} = r_{02} = r_{12} = 0$ . Equation (23) thus reduces to

$$\hat{\rho}_A = r(|0\rangle_j \langle 0| + |2\rangle_j \langle 2|) + (1 - 2r)|1\rangle_j \langle 1|. \quad (27)$$

Substituting Eq. (27) into Eq. (2), we find that the RE is proportional to the density of doublons (holons) as

$$S_A = -\log[2r^2 + (1 - 2r)^2] = 4r + \mathcal{O}((J/U)^4). \quad (28)$$

To see why excited doublons and holons yield entanglement, we expand the wave function (12) to the first order of  $J/U$  as

$$\begin{aligned} |\psi(t)\rangle &\sim |\psi_0\rangle + 2i(J/U) \sum_k \sin(k) [1 - e^{-i(\epsilon_{d,k} + \epsilon_{h,k})t}] \\ &\times \frac{\hat{d}_k^\dagger \hat{h}_{-k}^\dagger + \hat{h}_k^\dagger \hat{d}_{-k}^\dagger}{\sqrt{2}} |\psi_0\rangle. \end{aligned} \quad (29)$$

The second term illustrates that all the doublons and holons are excited as *entangled pairs* [22]. The RE quantifies entanglement between the subsystems A and B. It is proportional to the number of doublon-holon pairs spanning the boundary between the subsystems A and B. Since the density of doublons (holons) is equal to that of doublon-holon pairs, the RE is naturally proportional to the density of doublons (holons).

In the limit  $L \rightarrow \infty$ , evaluating the integrals in Eq. (26) by replacing the summation with the integral, we obtain

$$S_A(t) = 32(J/U)^2 \left[ 1 - \frac{\mathcal{J}_1(6Jt)}{3Jt} \cos(Ut) \right] + \mathcal{O}((J/U)^4), \quad (30)$$

where  $\mathcal{J}_n(x)$  is the Bessel function of the first kind. The density of doublon-holon pairs is indeed  $r(t) = S_A(t)/4$ .

The RE rapidly oscillates soon after the quench and saturates after a while, as shown in Fig. 2. The constant value after the saturation increases as  $J/U$  increases. Equation (30) shows that the frequency of the oscillation is equivalent to  $U$  and  $S_A$  saturates in the time scale of  $\mathcal{O}(1/J)$ . The constant after the saturation is given as

$$\lim_{t \rightarrow \infty} S_A = 32(J/U)^2 + \mathcal{O}((J/U)^4), \quad (31)$$

where the time-dependent part in Eq. (30) vanishes due to the dephasing effect. Figure 2 shows that Eqs. (30) and (31) agree well with the numerical results of the iTEBD calculations.

The Fourier transform of Eq. (30) is given as

$$\begin{aligned} \bar{S}_A(\omega) &= \int_{-\infty}^{\infty} dt S_A(t) e^{i\omega t} \\ &= -\frac{32J}{3U^2} \sqrt{1 - \left(\frac{U - \omega}{6J}\right)^2} \theta(6J - |\omega - U|), \end{aligned} \quad (32)$$

where  $\theta(x)$  is the step function. It has a peak at  $\omega = U$  that has the width  $\Delta\omega = 12J$ , as shown in the inset of Fig. 2. The rapid oscillations with the frequency  $U$  are induced by the excited bogolons in Eq. (12). Their excitation energy can be approximated as  $\epsilon_{d,k} + \epsilon_{h,k} \simeq U - 6J \cos(k)$  for  $J/U \ll 1$ . The peak position  $\omega = U$  corresponds to the center of the energy band, while the peak width  $12J$  corresponds to its band width.

### B. Rényi entropy for $L_A \geq 1$

The reduced density matrix for the time-evolving wave function  $|\psi(t)\rangle$  under the quadratic Hamiltonian  $H_{\text{eff}}$  can be formally written in the form of a thermal state as

$$\hat{\rho}_A = \text{tr}_B(|\psi(t)\rangle\langle\psi(t)|) = \frac{e^{-\hat{\mathcal{H}}_A}}{\text{tr}(e^{-\hat{\mathcal{H}}_A})}, \quad (33)$$

where  $\hat{\mathcal{H}}_A(t)$  is a quadratic Hamiltonian of  $\hat{d}_j$  and  $\hat{h}_j$  ( $j \in A$ ) [We summarize the derivation of Eq. (33) in Appendix C]. Following the formalism in Appendix B, the matrix of the single-particle correlation functions  $M$  can be written in the form of Eq. (15). We thus obtain

$$S_A = 4 \left[ \text{tr}(C) - \|F\|_F^2 \right] + \mathcal{O}((J/U)^4), \quad (34)$$

where the  $(i, j)$  ( $i, j \in A$ ) elements of the  $L_A \times L_A$  matrices  $C$  and  $F$  are given, respectively, as

$$\begin{aligned} C_{ij} &= \langle \psi(t) | \hat{d}_i^\dagger \hat{d}_j | \psi(t) \rangle = \langle \psi(t) | \hat{h}_i^\dagger \hat{h}_j | \psi(t) \rangle, \\ &= \frac{2}{L} \sum_k u_k^2 v_k^2 \{1 - \cos[(\epsilon_{d,k} + \epsilon_{h,k})t]\} e^{i(i-j)k}, \end{aligned} \quad (35)$$

$$\begin{aligned} F_{ij} &= \langle \psi(t) | \hat{d}_i \hat{h}_j | \psi(t) \rangle = \langle \psi(t) | \hat{h}_i \hat{d}_j | \psi(t) \rangle, \\ &= \frac{i}{L} \sum_k u_k v_k e^{ik(i-j)} \\ &\times \left[ v_k^2 (1 - e^{i(\epsilon_{d,k} + \epsilon_{h,k})t}) - u_k^2 (1 - e^{-i(\epsilon_{d,k} + \epsilon_{h,k})t}) \right]. \end{aligned} \quad (36)$$

Note that  $C_{ii} = r(t)$  and  $F_{ii} = 0$ .

In the limit  $L \rightarrow \infty$ , evaluating the summation in Eq. (36), we obtain

$$\begin{aligned} F_{i,i+n} &= \sqrt{2}(J/U)(\delta_{n,1} - \delta_{n,-1}) \\ &+ \sqrt{2}(J/U)i^{n+1}e^{-iUt}n \frac{\mathcal{J}_n(6Jt)}{3Jt} + \mathcal{O}((J/U)^2), \end{aligned} \quad (37)$$

$$\begin{aligned} \|F\|_F^2 &= 4(J/U)^2(L_A - 1) \\ &+ 4(J/U)^2 \left\{ \sum_{n=0}^{L_A-1} (L_A - n)n^2 \left( \frac{\mathcal{J}_n(6Jt)}{3Jt} \right)^2 \right. \\ &\left. - 2(L_A - 1) \frac{\mathcal{J}_1(6Jt)}{3Jt} \cos(Ut) \right\} + \mathcal{O}((J/U)^3). \end{aligned} \quad (38)$$

$C_{ii} = r(t) = S_A(t)/4$  can be obtained from Eq. (30). The

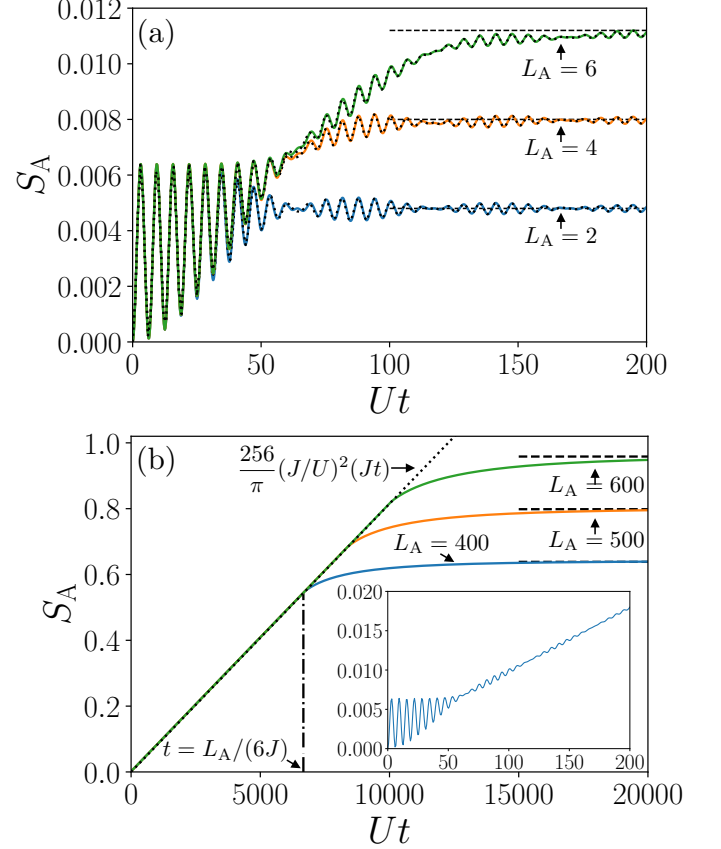


FIG. 3. Time evolution of the RE for  $L_A \geq 1$ . We set  $J/U = 0.01$ . Equation (39) is plotted as the solid lines. The dashed lines indicate  $16(J/U)^2(L_A + 1)$ . (a) RE for  $1 \leq L_A \leq 6$  in the short-time scale. The numerical results of the iTEBD algorithm are indicated by the dotted lines. (b) RE for  $L_A = 400, 500$ , and  $600$  in the long-time scale. The inset shows a magnification in the short-time scale.

RE for  $L_A \geq 1$  is given as

$$\begin{aligned} S_A(t) &= 16 \left( \frac{J}{U} \right)^2 (L_A + 1) - 32 \left( \frac{J}{U} \right)^2 \cos(Ut) \frac{\mathcal{J}_1(6Jt)}{3Jt} \\ &- 16 \left( \frac{J}{U} \right)^2 \sum_{n=0}^{L_A} (L_A - n)n^2 \left( \frac{\mathcal{J}_n(6Jt)}{3Jt} \right)^2 + \mathcal{O}((J/U)^3). \end{aligned} \quad (39)$$

Setting  $L_A = 1$ , the above equation indeed reduces to Eq. (30).

Figures 3 (a) and (b) show  $S_A(t)$  in Eq. (39) as functions of time in the short-time scale for a small subsystem [ $Jt, L_A = \mathcal{O}(1)$ ] and long-time scale for a large subsystem [ $Jt, L_A \gg 1$ ], respectively. The numerical results of the iTEBD calculations agree well with Eq. (39), as shown in Fig. 3 (a). Analogous to Fig. 2,  $S_A(t)$  exhibits the rapid oscillations with the frequency  $U$  and the saturation in the time scale of  $\mathcal{O}(1/J)$ . Meanwhile, in Fig. 3 (b), we

find that  $S_A$  linearly increases for  $6Jt < L_A$  and saturates to a constant that is proportional to the size of the subsystem  $L_A$  for  $6Jt > L_A$ , i.e., it obeys the *volume-law scaling*. We can confirm these behaviors analytically as

$$\lim_{t \rightarrow \infty} \left( \lim_{L_A \rightarrow \infty} S_A \right) = 256 \left( \frac{J}{U} \right)^2 \frac{Jt}{\pi} + \mathcal{O}((J/U)^3), \quad (40)$$

$$\lim_{L_A \rightarrow \infty} \left( \lim_{t \rightarrow \infty} S_A \right) = 16(J/U)^2 L_A + \mathcal{O}((J/U)^3). \quad (41)$$

Note that the oscillations with the frequency  $U$  can be seen in the short-time scale, as shown in the inset of Fig. 3 (b).

## VI. QUASIPARTICLE PICTURE

We argue the physical picture for the time evolution of  $S_A(t)$  based on the doublon-holon quasiparticle picture. First of all, we describe a physical interpretation of Eq. (34).  $\text{tr}(C) = \sum_{j \in A} (\langle \hat{n}_{jd} \rangle + \langle \hat{n}_{jh} \rangle)$  represents the total number of doublons and holons in the subsystem A, which is equal to the sum of the number of doublon-holon pairs spanning the boundary of the subsystem A and two times the number of doublon-holon pairs within the subsystem A [See Fig. 4 (a)], while  $\|F\|_F^2 = \sum_{i,j \in A} |\langle \hat{d}_i \hat{h}_j \rangle|^2$  is equal to two times the number of pairs within A [Fig. 4 (b)].  $\text{tr}(C) - \|F\|_F^2$  is, therefore, equal to the number of entangled doublon-holon pairs spanning the boundary of A [Fig. 4 (c)]. It naturally describes the entanglement between the subsystems A and B.

Figure 5 (a) shows  $|F_{i,i+n}(t)|^2$  as a function of  $n$ . The propagating peaks in the figure correspond to those of the Bessel function  $\mathcal{J}_n(6Jt)$  ( $1 \leq n \leq L_A - 1$ ) in Eq. (38). Each of them describes a wave packet of an entangled doublon-holon pair emitted by the quench. The most dominant peak of  $\mathcal{J}_n(6Jt)$  at  $n = 6Jt$  represents a pair emitted at the initial time  $t = 0$ . The sub-dominant propagating peaks represent the pairs emitted later ( $t > 0$ ). All the peaks propagate with the same velocity  $v_{\text{pair}} = 6J$ , which coincides with the maximum group velocity of a doublon-holon pair with opposite momenta as

$$v_{\text{pair}} = \max[\partial_k(\epsilon_{d,k} + \epsilon_{h,-k})] \sim 6J. \quad (42)$$

This propagation speed of doublon-holon pairs has been experimentally confirmed by measuring the correlation functions [22]. These pairs decay as shown in Fig. 5 (a) due to the factor  $3Jt$  in the denominator of the second term in the bracket of Eq. (38).

To figure out the physical picture for the characteristic features of the long-time dynamics, namely, the linear growth for  $6Jt < L_A$  and the following saturation for  $6Jt > L_A$ , we focus on the matrix  $|F_{i,j}(t)|^2$  that is visualized in Fig. 5 (b). One finds that, when  $6Jt < L_A$ , the contribution of the pair emitted at  $t = 0$  decreases as the size of the pair grows. It leads to the linear growth

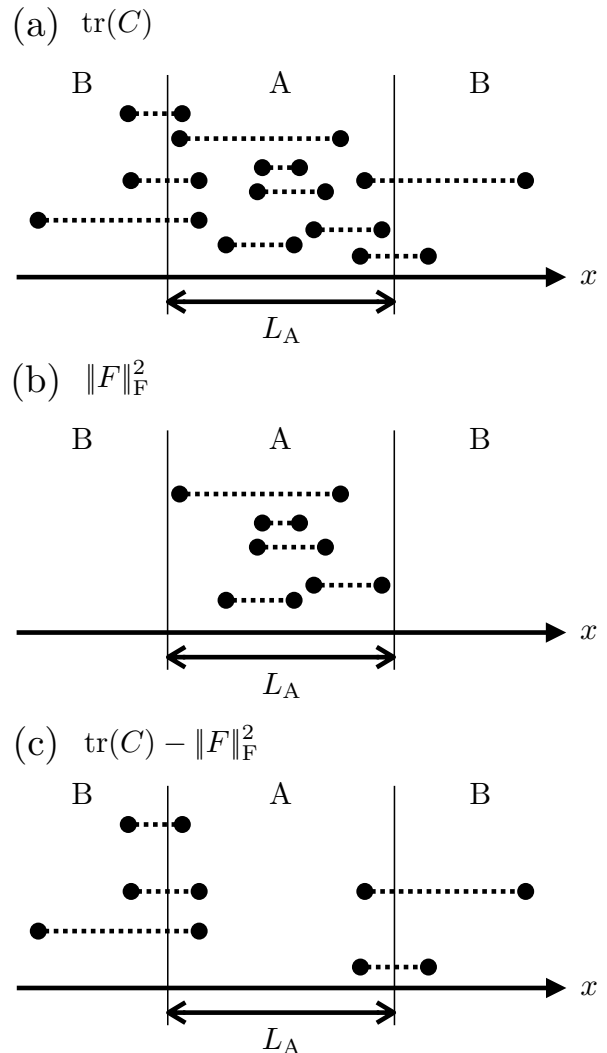


FIG. 4. Schematic drawings describing the physical image of (a)  $\text{tr}(C)$ , (b)  $\|F\|_F^2$ , and (c)  $\text{tr}(C) - \|F\|_F^2$ . Each two dots connected by a dotted line represents an entangled pair of a doublon and a holon.

of  $S_A(t)$  for  $6Jt < L_A$ . When  $6Jt > L_A$ , the pair emitted at  $t = 0$  spreads beyond the subsystem size and its contribution to  $\|F\|_F^2$  disappears. This results in the saturation of  $S_A$ . The smooth transition from the linear growth to the saturation of  $S_A$  is due to the contribution of the sub-dominant peaks, i.e., pairs emitted at  $t > 0$ .

In addition to the propagating peaks, there is a single localized peak at  $n = 1$  in Fig. 5 (a) that corresponds to the subdiagonal elements in Fig. 5 (b). It arises from the second term in Eq. (39), so its height oscillates with the frequency  $U$ . This localized peak represents the doublon-holon pairs with a unit separation spanning the boundary of A. They are excited by hopping of a boson to the next-nearest sites. They repeat creation and annihilation with the frequency  $U$  and eventually decay.

Calabrese and Cardy proposed a quasiparticle picture for the quench dynamics of integrable systems in the

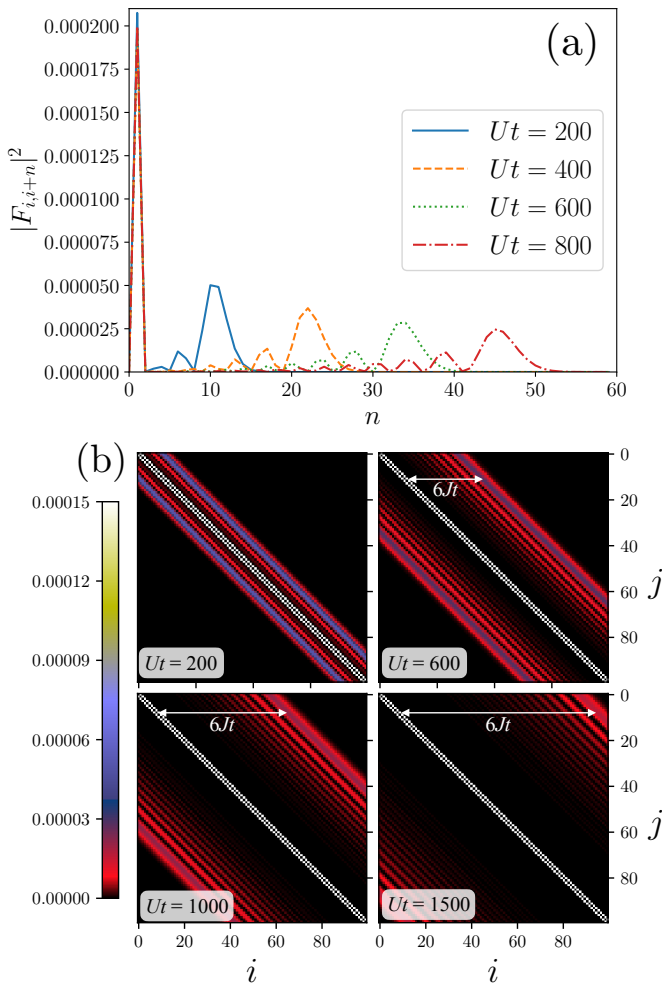


FIG. 5. (a)  $|F_{i,i+n}(t)|^2$  as a function of  $n$ . (b) Colormap of  $|F_{ij}(t)|^2$ . We set  $J/U = 0.01$  in both (a) and (b).

study of the transverse-field Ising model [18]. Comparing it with the above physical picture, we find a few differences between them. First, Ref. [18] only refers to the entangled pairs emitted at  $t = 0$ . We find that pairs emitted later time  $t > 0$  play roles in the dynamics of entanglement entropy. In particular, the smooth transition from the linear growth to the saturation of  $S_A$  can be explained by their contribution. Second, we find that the doublon-holon pairs decay as they propagate. Third, the localized doublon-holon pairs with a unit separation spanning the boundary of the subsystem yield the rapid oscillation of  $S_A$  in the short-time dynamics. Besides these differences, our physical picture is consistent with that of Ref. [18].

## VII. DISCUSSION

We make a few final remarks in this section as for 1) the validity of the effective theory and 2) the verifiability

of our results in experiments: 1) In deriving the effective Hamiltonian (4), we neglect the projection operator that eliminates the fictitious states with a doublon and a holon on the same site (See Appendix A). Since the effective Hamiltonian with the projection operator is non-integrable, we expect that thermalization occurs. If this is the case, the non-integrability effect is very small because it is proportional to the square of the density of doublons and holons. As a result, thermalization would be realized over a very long time. This means that the saturation of the RE may be a transient phenomenon. The RE may grow again after a long time and approach the Page value for the spin-1 chain in Eq. (A4) [39, 40] or that of BHM [41–44].

2) It may be difficult to experimentally confirm our predictions on the long-time dynamics of the RE due to the limitation of the lifetime of an atomic gas and the finite size effect. The short-time dynamics of the RE in Fig. 3 (a) may be verifiable using the experimental setup in Refs. [20, 21].

## ACKNOWLEDGMENTS

We thank I. Danshita, R. Kaneko, K. Sugiyama, and Y. Takeuchi for fruitful discussions. ST thanks D. Huerga and R. Raussendorf for stimulating discussions. SY is supported by Grant-in-Aid for JSPS Fellows (Grant No. JP22J22306). DK was supported by JST CREST (Grant No. JPMJCR1673) and JST FOREST (Grant No. JPMJFR202T). RY is partially supported by a Grant-in-Aid of MEXT for Scientific Research KAKENHI (Grant Nos. 19K14616 and 20H01838). ST is supported by the Japan Society for the Promotion of Science Grant-in-Aid for Scientific Research (KAKENHI Grant No. 19K03691).

## Appendix A: Derivation of the effective Hamiltonian

We give the derivation of the effective Hamiltonian from the BHM in this Appendix. When  $J/U$  is sufficiently small, the system can be mapped to a spin-1 system as it can be effectively described within the truncated Hilbert space spanned by  $|0\rangle_j$ ,  $|1\rangle_j$ , and  $|2\rangle_j$ , where they correspond to the spin-1 states:  $|2\rangle_j = |S_z = 1\rangle_j$ ,  $|1\rangle_j = |S_z = 0\rangle_j$ , and  $|0\rangle_j = |S_z = -1\rangle_j$  [45]. Introducing the spin-1 operators

$$\hat{S}_j^+ = \sqrt{2}(|S_z = 1\rangle_j \langle S_z = 0| + |S_z = 0\rangle_j \langle S_z = -1|), \quad (\text{A1})$$

$$\hat{S}_j^- = \sqrt{2}(|S_z = 0\rangle_j \langle S_z = 1| + |S_z = -1\rangle_j \langle S_z = 0|), \quad (\text{A2})$$

$$\hat{S}_j^z = |S_z = 1\rangle_j \langle S_z = 1| - |S_z = -1\rangle_j \langle S_z = -1|, \quad (\text{A3})$$

the BHM (1) can be written as

$$\begin{aligned} \hat{H} = & -\frac{J}{2} \sum_j [\hat{S}_j^+ \hat{S}_j^z \hat{S}_{j+1}^z \hat{S}_{j+1}^- + 2\hat{S}_j^z \hat{S}_j^+ \hat{S}_{j+1}^- \hat{S}_{j+1}^z \\ & - \sqrt{2}(\hat{S}_j^+ \hat{S}_j^z \hat{S}_{j+1}^- \hat{S}_{j+1}^z + \hat{S}_j^z \hat{S}_j^+ \hat{S}_{j+1}^z \hat{S}_{j+1}^-) + \text{h.c.}] \\ & + \frac{U}{2} \sum_j \hat{S}_j^{z2} + \frac{U}{2} \sum_j \hat{S}_j^z. \end{aligned} \quad (\text{A4})$$

Since  $\sum_j \hat{S}_j^z = \sum_j (\hat{n}_j - 1) = N - L$  is a constant, we neglect the last term in Eq. (A4).

We introduce the pseudo-fermion operators  $\bar{d}_j$  and  $\bar{h}_j$  by the generalized Jordan-Wigner transformation [46]

$$\hat{S}_j^+ = \sqrt{2}(\bar{d}_j^\dagger + \bar{h}_j) \hat{K}_j, \quad (\text{A5})$$

$$\hat{S}_j^- = \sqrt{2}(\bar{d}_j + \bar{h}_j^\dagger) \hat{K}_j, \quad (\text{A6})$$

$$\hat{S}_j^z = \bar{n}_{jd} - \bar{n}_{jh}, \quad (\text{A7})$$

where  $\bar{n}_{jd} = \bar{d}_j^\dagger \bar{d}_j$ ,  $\bar{n}_{jh} = \bar{h}_j^\dagger \bar{h}_j$ , and  $\hat{K}_j = \prod_{i<j} (1 - 2\bar{n}_{id})(1 - 2\bar{n}_{ih}) = \prod_{i<j} (-1)^{(\hat{S}_i^z)^2}$  is the string operator. The inverse transformation is given by

$$\bar{d}_j = \frac{1}{\sqrt{2}} \hat{K}_j \hat{S}_j^- \hat{S}_j^z, \quad (\text{A8})$$

$$\bar{h}_j = -\frac{1}{\sqrt{2}} \hat{K}_j \hat{S}_j^+ \hat{S}_j^z. \quad (\text{A9})$$

$\bar{d}_j$  and  $\bar{h}_j$  are annihilation operators of ‘‘particle’’ and ‘‘hole’’ excitations, respectively, because  $\bar{d}_j|1\rangle_j = \bar{h}_j|1\rangle_j = 0$ ,  $|2\rangle_j = \hat{K}_j \bar{d}_j^\dagger|1\rangle_j \propto \bar{d}_j^\dagger|1\rangle_j$ , and  $|0\rangle_j = \hat{K}_j \bar{h}_j^\dagger|1\rangle_j \propto \bar{h}_j^\dagger|1\rangle_j$ . However, since their multiple occupation on the same site is prohibited ( $\bar{d}_j^\dagger \bar{h}_j^\dagger = 0$ ), they do not obey the fermionic anti-commutation relations. Note that the string operator  $\hat{K}_j$  gives a phase factor that depends on  $(\hat{S}_i^z)^2$  ( $1 \leq i \leq j-1$ ).

We further introduce the annihilation operators  $\hat{d}_j$  and  $\hat{h}_j$  as

$$\bar{d}_j = (1 - \hat{n}_{jh}) \hat{d}_j, \quad (\text{A10})$$

$$\bar{h}_j = (1 - \hat{n}_{jd}) \hat{h}_j, \quad (\text{A11})$$

where  $\hat{n}_{jd} = \hat{d}_j^\dagger \hat{d}_j$  and  $\hat{n}_{jh} = \hat{h}_j^\dagger \hat{h}_j$ . They represent fermionic excitations as they satisfy the usual anti-commutation relations:  $\{\hat{d}_i, \hat{d}_j^\dagger\} = \{\hat{h}_i, \hat{h}_j^\dagger\} = \delta_{i,j}$ ,  $\{\hat{d}_i, \hat{d}_j\} = \{\hat{h}_i, \hat{h}_j\} = \{\hat{d}_i, \hat{h}_j\} = \{\hat{d}_i, \hat{h}_j^\dagger\} = 0$ . We obtain  $|0\rangle_j = |n_d = 0, n_h = 1\rangle_j$ ,  $|1\rangle_j = |n_d = 0, n_h = 0\rangle_j$ , and  $|2\rangle_j = |n_d = 1, n_h = 0\rangle_j$  from  $\hat{S}_j^z = \hat{n}_{jd} - \hat{n}_{jh}$ .  $\hat{d}_j$  and  $\hat{h}_j$  thus describe fermionic particle and hole excitations, respectively. We refer to them as ‘‘doublon’’ and ‘‘holon’’ in this paper. Note that  $|1\rangle_j = |n_d = 0, n_h = 0\rangle_j$  is the vacuum of  $\hat{d}_j$  and  $\hat{h}_j$ .  $|n_d = 1, n_h = 1\rangle_j$  has no corresponding Fock states of original bosons.

Substituting Eqs. (A5)-(A11) into Eq. (A4), we obtain

$$\hat{H} = \hat{P} \hat{H}_{\text{eff}} \hat{P}, \quad (\text{A12})$$

where  $\hat{H}_{\text{eff}}$  is given in Eq. (4). The projection operator  $\hat{P} = \prod_j (1 - \hat{n}_{jd} \hat{n}_{jh})$  eliminates the state  $|n_d = 1, n_h = 1\rangle_j$ . The projection operator can be safely neglected in weakly excited states of the deep MI regime, since the system can be considered as a dilute gas of doublons and holons and the possibility of their occupation on the same site is quite low.

By the Fourier transform

$$\hat{d}_j = \frac{1}{\sqrt{L}} \sum_k e^{ikj} \hat{d}_k, \quad (\text{A13})$$

$$\hat{h}_j = \frac{1}{\sqrt{L}} \sum_k e^{ikj} \hat{h}_k, \quad (\text{A14})$$

we obtain

$$\begin{aligned} \hat{H}_{\text{eff}} = & \sum_k [f_{d,k} \hat{d}_k^\dagger \hat{d}_k - f_{h,k} \hat{h}_{-k} \hat{h}_{-k}^\dagger \\ & - ig_k (\hat{d}_k^\dagger \hat{h}_{-k}^\dagger - \hat{h}_{-k} \hat{d}_k)], \end{aligned} \quad (\text{A15})$$

where  $f_{d,k} = U/2 - 4J \cos(k)$  and  $f_{h,k} = U/2 - 2J \cos(k)$ ,  $g_k = 2\sqrt{2}J \sin(k)$ . Doublon and holon have energy gap  $f_{d,k=0} = U/2 - 4J$  and  $f_{h,k=0} = U/2 - 2J$ , respectively.

## Appendix B: Rényi entropy of a Gaussian state

We summarize the calculation of RE for a Gaussian state in this Appendix. The reduced density matrix for a Gaussian state  $|\phi\rangle$  can be formally written as [36]

$$\hat{\rho}_A = \text{tr}_B(|\phi\rangle\langle\phi|) = \frac{e^{-\hat{\mathcal{H}}_A}}{\text{tr}(e^{-\hat{\mathcal{H}}_A})}. \quad (\text{B1})$$

The entanglement Hamiltonian  $\hat{\mathcal{H}}_A$  has a quadratic form of  $\hat{d}_j$  and  $\hat{h}_j$  ( $j \in A$ ) and therefore it can be diagonalized as

$$\hat{\mathcal{H}}_A = \sum_{\alpha=1}^{2L_A} \omega_\alpha^A \hat{n}_\alpha^A, \quad (\text{B2})$$

where  $\omega_\alpha$  and  $\hat{n}_\alpha$  are the spectrum and the number operator for the eigenmode  $\alpha$ , respectively. Using Eq. (B1), we obtain

$$S_A = - \sum_{\alpha=1}^{2L_A} \log[1 - 2\{f_\alpha - (f_\alpha)^2\}], \quad (\text{B3})$$

where  $f_\alpha = \text{tr}_A(\hat{\rho}_A \hat{n}_\alpha) = 1/[\exp(\omega_\alpha^A) + 1]$  is the occupation number of the eigenmode  $\alpha$ .

We consider the matrix of single-particle correlation functions

$$M = \begin{pmatrix} I - C_{dd}^* & -C_{dh}^* & F_{dd} & F_{dh} \\ -C_{hd}^* & I - C_{hh}^* & F_{hd} & F_{hh} \\ -F_{dd}^* & -F_{dh}^* & C_{dd} & C_{dh} \\ -F_{hd}^* & -F_{hh}^* & C_{hd} & C_{hh} \end{pmatrix}, \quad (\text{B4})$$

Here,  $C_{\sigma\sigma'}$  and  $F_{\sigma\sigma'}$  ( $\sigma, \sigma' = d, h$ ) are  $L_A \times L_A$  matrices with the matrix elements

$$[C_{\sigma\sigma'}]_{ij} = \langle \phi | \hat{c}_{i\sigma}^\dagger \hat{c}_{j\sigma'} | \phi \rangle, \quad (\text{B5})$$

$$[F_{\sigma\sigma'}]_{ij} = \langle \phi | \hat{c}_{i\sigma} \hat{c}_{j\sigma'} | \phi \rangle, \quad (\text{B6})$$

where we denote  $\hat{c}_{id} = \hat{d}_i$  and  $\hat{c}_{ih} = \hat{h}_i$ .  $f_\alpha$  can be obtained by diagonalizing  $M$ , thanks to the relation [36]

$$M = U_A \begin{pmatrix} \text{diag}(1 - f_\alpha) & 0 \\ 0 & \text{diag}(f_\alpha) \end{pmatrix} U_A^{-1}, \quad (\text{B7})$$

where  $U_A$  is a unitary matrix.

### Appendix C: Derivation of Eq. (33)

In this Appendix, we give the derivation of Eq. (33). The following arguments is based on Ref. [36].

Let us consider a many-body correlation function  $\langle \psi(t) | \hat{a}_{i_1} \hat{a}_{i_2}, \dots, \hat{a}_{i_{2n}} | \psi(t) \rangle$ , where  $\hat{a}_i \in \{\hat{d}_i, \hat{h}_i, \hat{d}_i^\dagger, \hat{h}_i^\dagger\}$ . In the Heisenberg picture, it can be written as

$$\langle \psi_0 | \check{a}_{i_1}(t) \check{a}_{i_2}(t) \dots \check{a}_{i_{2n}}(t) | \psi_0 \rangle, \quad (\text{C1})$$

where  $\check{a}_i(t) = e^{iH_{\text{eff}}t} \hat{a}_i e^{-iH_{\text{eff}}t}$ . Since  $\hat{H}_{\text{eff}}$  is a quadratic Hamiltonian of  $\{\hat{a}_i\}$ ,  $\check{a}_i(t)$  can be represented by a linear combination of  $\{\hat{a}_i\}$ . Given that  $|\psi_0\rangle$  is the vacuum of  $\hat{d}_j$  and  $\hat{h}_j$ , Eq. (C1) can be decomposed into one-body correlation functions by Wick's theorem [47]. We thus

obtain

$$\begin{aligned} & \langle \psi_0 | \check{a}_{i_1}(t) \check{a}_{i_2}(t), \dots, \check{a}_{i_{2n-1}}(t) \check{a}_{i_{2n}}(t) | \psi_0 \rangle = \\ & \sum_{\sigma \in P} \text{sgn}(\sigma) \langle \psi_0 | \check{a}_{j_1}(t) \check{a}_{j_2}(t) | \psi_0 \rangle \langle \psi_0 | \check{a}_{j_3}(t) \check{a}_{j_4}(t) | \psi_0 \rangle \dots \\ & \times \langle \psi_0 | \check{a}_{j_{2n-3}}(t) \check{a}_{j_{2n-2}}(t) | \psi_0 \rangle \langle \psi_0 | \check{a}_{j_{2n-1}}(t) \check{a}_{j_{2n}}(t) | \psi_0 \rangle, \end{aligned} \quad (\text{C2})$$

where  $P$  is the set of permutations  $(i_1, i_2, \dots, i_{2n} \rightarrow j_1, j_2, \dots, j_{2n})$  satisfying  $j_{k-1} < j_k$  and  $j_1 < j_3 < \dots < j_{2n-1}$ . Returning to the Schrödinger picture, Eq. (C2) becomes

$$\langle \psi(t) | \hat{a}_{i_1} \hat{a}_{i_2}, \dots, \hat{a}_{i_{2n-1}} \hat{a}_{i_{2n}} | \psi(t) \rangle =$$

$$\sum_{\sigma \in P} \text{sgn}(\sigma) \langle \psi(t) | \hat{a}_{j_1} \hat{a}_{j_2} | \psi(t) \rangle \langle \psi(t) | \hat{a}_{j_3} \hat{a}_{j_4} | \psi(t) \rangle \dots$$

$$\times \langle \psi(t) | \hat{a}_{j_{2n-3}} \hat{a}_{j_{2n-2}} | \psi(t) \rangle \langle \psi(t) | \hat{a}_{j_{2n-1}} \hat{a}_{j_{2n}} | \psi(t) \rangle. \quad (\text{C3})$$

If the many-body correlation function (C1) concerns the degrees of freedom in the subsystem A, i.e.,  $\{i_1, i_2, \dots, i_{2n}\} \in A$ , all the correlation functions in Eq. (C3) can be calculated by the reduced density matrix for A. In this case, Eq. (C3) can be written as

$$\begin{aligned} \text{tr}_A(\hat{\rho}_A \hat{a}_{i_1} \hat{a}_{i_2}, \dots, \hat{a}_{i_{2n}}) &= \sum_{\sigma \in P} \text{sgn}(\sigma) \text{tr}_A(\hat{\rho}_A \hat{a}_{j_1} \hat{a}_{j_2}) \\ &\times \text{tr}_A(\hat{\rho}_A \hat{a}_{j_3} \hat{a}_{j_4}) \dots \text{tr}_A(\hat{\rho}_A \hat{a}_{j_{2n-1}} \hat{a}_{j_{2n}}). \end{aligned} \quad (\text{C4})$$

Equation (C4) shows that the Bloch-De Dominicis theorem [48] can be applied to the correlation functions evaluated by  $\hat{\rho}_A$ . It follows that  $\hat{\rho}_A$  is a thermal state of a quadratic Hamiltonian of  $\hat{d}_j$  and  $\hat{h}_j$  ( $j \in A$ ). We thus obtain Eq. (33).

- 
- [1] A. Einstein, B. Podolsky, and N. Rosen, Phys. Rev. **47**, 777 (1935).  
[2] J. S. Bell, Physics Physique Fizika **1**, 195 (1964).  
[3] J. M. Deutsch, Phys. Rev. A **43**, 2046 (1991).  
[4] M. Srednicki, Phys. Rev. E **50**, 888 (1994).  
[5] H. Tasaki, Phys. Rev. Lett. **80**, 1373 (1998).  
[6] T. Kinoshita, T. Wenger, and D. S. Weiss, Nature **440**, 900 (2006).  
[7] M. Rigol, V. Dunjko, and M. Olshanii, Nature **452**, 854 (2008).  
[8] R. Yoshii, S. Yamashika, and S. Tsuchiya, Journal of the Physical Society of Japan **91**, 054601 (2022).  
[9] S. W. Hawking, Nature **248**, 30 (1974).  
[10] S. W. Hawking, in *Euclidean quantum gravity* (World Scientific, 1975) pp. 167–188.  
[11] R. Raussendorf and H. J. Briegel, Phys. Rev. Lett. **86**, 5188 (2001).  
[12] A. Kitaev, Annals of Physics **303**, 2 (2003).  
[13] M. Fagotti and P. Calabrese, Phys. Rev. A **78**, 010306 (2008).  
[14] V. Alba and P. Calabrese, Proceedings of the National Academy of Sciences **114**, 7947 (2017).  
[15] V. Alba and P. Calabrese, Phys. Rev. B **96**, 115421 (2017).  
[16] B. Bertini, K. Klobas, V. Alba, G. Lagnese, and P. Calabrese, Phys. Rev. X **12**, 031016 (2022).  
[17] P. Calabrese and J. Cardy, Journal of Statistical Mechanics: Theory and Experiment **2004**, P06002 (2004).  
[18] P. Calabrese and J. Cardy, Journal of Statistical Mechanics: Theory and Experiment **2005**, P04010 (2005).  
[19] A. J. Daley, H. Pichler, J. Schachenmayer, and P. Zoller, Phys. Rev. Lett. **109**, 020505 (2012).  
[20] R. Islam, R. Ma, P. M. Preiss, M. Eric Tai, A. Lukin, M. Rispoli, and M. Greiner, Nature **528**, 77 (2015).  
[21] A. M. Kaufman, M. E. Tai, A. Lukin, M. Rispoli, R. Schittko, P. M. Preiss, and M. Greiner, Science **353**,

- 794 (2016).
- [22] M. Cheneau, P. Barmettler, D. Poletti, M. Endres, P. Schauß, T. Fukuhara, C. Gross, I. Bloch, C. Kollath, and S. Kuhr, *Nature* **481**, 484 (2012).
- [23] M. P. A. Fisher, P. B. Weichman, G. Grinstein, and D. S. Fisher, *Phys. Rev. B* **40**, 546 (1989).
- [24] D. Jaksch, C. Bruder, J. I. Cirac, C. W. Gardiner, and P. Zoller, *Phys. Rev. Lett.* **81**, 3108 (1998).
- [25] S. Sachdev, *Quantum phase transitions* (Cambridge university press, 2011).
- [26] G. G. Batrouni, R. T. Scalettar, and G. T. Zimanyi, *Phys. Rev. Lett.* **65**, 1765 (1990).
- [27] V. A. Kashurnikov and B. V. Svistunov, *Phys. Rev. B* **53**, 11776 (1996).
- [28] T. D. Kühner and H. Monien, *Phys. Rev. B* **58**, R14741 (1998).
- [29] I. Danshita and A. Polkovnikov, *Phys. Rev. A* **84**, 063637 (2011).
- [30] S. Ejima, H. Fehske, and F. Gebhard, *EPL (Europhysics Letters)* **93**, 30002 (2011).
- [31] J. Carrasquilla, S. R. Manmana, and M. Rigol, *Phys. Rev. A* **87**, 043606 (2013).
- [32] K. V. Krutitsky, *Physics Reports* **607**, 1 (2016).
- [33] R. Horodecki, P. Horodecki, M. Horodecki, and K. Horodecki, *Rev. Mod. Phys.* **81**, 865 (2009).
- [34] M. Nakahara, *Quantum computing: from linear algebra to physical realizations* (CRC press, 2008).
- [35] J. Bardeen, L. N. Cooper, and J. R. Schrieffer, *Phys. Rev.* **106**, 162 (1957).
- [36] I. Frérot and T. Roscilde, *Phys. Rev. B* **92**, 115129 (2015).
- [37] J. Eisert, M. Cramer, and M. B. Plenio, *Rev. Mod. Phys.* **82**, 277 (2010).
- [38] R. Orús and G. Vidal, *Phys. Rev. B* **78**, 155117 (2008).
- [39] M. Schecter and T. Iadecola, *Phys. Rev. Lett.* **123**, 147201 (2019).
- [40] S. Chattopadhyay, H. Pichler, M. D. Lukin, and W. W. Ho, *Phys. Rev. B* **101**, 174308 (2020).
- [41] D. N. Page, *Phys. Rev. Lett.* **71**, 1291 (1993).
- [42] A. Russomanno, M. Fava, and R. Fazio, *Phys. Rev. B* **102**, 144302 (2020).
- [43] M. Kunimi and I. Danshita, *Phys. Rev. A* **104**, 043322 (2021).
- [44] D. Kagamihara, R. Kaneko, S. Yamashika, K. Sugiyama, R. Yoshii, S. Tsuchiya, and I. Danshita, *arXiv preprint arXiv:2207.08353* (2022).
- [45] E. Altman and A. Auerbach, *Phys. Rev. Lett.* **89**, 250404 (2002).
- [46] C. D. Batista and G. Ortiz, *Phys. Rev. Lett.* **86**, 1082 (2001).
- [47] G. C. Wick, *Phys. Rev.* **80**, 268 (1950).
- [48] T. Matsubara, *Progress of Theoretical Physics* **14**, 351 (1955).